Neural Matching Fields: Implicit Representation of Matching Fields for Visual Correspondence

Sunghwan Hong Korea University
Jisu Nam Korea University
Seokju Cho Korea University
Susung Hong Korea University
Sangryul Jeon UC Berkeley
Dongbo Min Ewha Womans University
Seungryong Kim[*] Korea University

Abstract

Existing pipelines of semantic correspondence commonly include extracting high-level semantic features for the invariance against intra-class variations and background clutters. This architecture, however, inevitably results in a low-resolution matching field that additionally requires an ad-hoc interpolation process as a post-processing for converting it into a high-resolution one, certainly limiting the overall performance of matching results. To overcome this, inspired by recent success of implicit neural representation, we present a novel method for semantic correspondence, called Neural Matching Field (NeMF). However, complicacy and high-dimensionality of a 4D matching field are the major hindrances, which we propose a cost embedding network to process a coarse cost volume to use as a guidance for establishing high-precision matching field through the following fully-connected network. Nevertheless, learning a high-dimensional matching field remains challenging mainly due to computational complexity, since a naïve exhaustive inference would require querying from all pixels in the 4D space to infer pixel-wise correspondences. To overcome this, we propose adequate training and inference procedures, which in the training phase, we randomly sample matching candidates and in the inference phase, we iteratively performs PatchMatch-based inference and coordinate optimization at test time. With these combined, competitive results are attained on several standard benchmarks for semantic correspondence. Code and pre-trained weights are available at `https://ku-cvlab.github.io/NeMF/`.

1 Introduction

Establishing visual correspondence across semantically similar images is a fundamental problem in computer vision, which has been facilitating many applications including visual localization [68, 38], structure-from-motion [69], image editing [1] and autonomous driving [33]. Unlike traditional dense correspondence tasks [20, 23], where visually similar images of the same scene are used as inputs, semantic correspondence problem poses additional challenges due to intra-class appearance and severe geometry variations among object instances [15, 16].

Much research [65, 48, 29, 25, 32, 50, 64, 26, 47, 31, 8, 35, 77, 9] in semantic correspondence literature attempt to address above challenges by leveraging Convolutional Neural Networks (CNNs)-based features thanks to their greater semantic invariance than traditional hand-crafted descriptors [37, 10, 66, 3] that only capture low-level local structure. As shown in Fig. 1(a), they typically perform matching with deeper features that contain high-level semantics to obtain a low-resolution correspondence map, and they are enforced to use hand-crafted interpolation techniques, *e.g.,* bilinear

[*]Corresponding author

36th Conference on Neural Information Processing Systems (NeurIPS 2022).

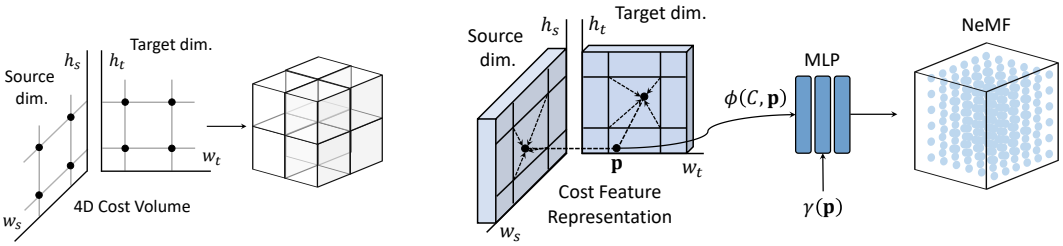

(a) Existing works (b) NeMF (Ours)

Figure 1: **Intuition of the proposed neural matching field (NeMF):** (a) existing works [47, 8] and (b) the proposed NeMF. Unlike existing methods that explicitly compute and store discrete matching field defined at low resolution, we implicitly represent a high-dimensional 4D matching field with deep fully-connected networks defined at arbitrary original image resolution.

interpolation [65, 64, 26, 8, 77, 9] or TPS warping with sparse keypoints [48, 50, 47], significantly reducing localization precision in matching details. Instead of these hand-crafted designs, several works [25, 76, 19] attempted to formulate a coarse-to-fine approach by utilizing multi-level features, but they often suffer from the propagation of initial error from the early coarse level.

Inspired by recent success of Implicit Neural Representation (INR) [44, 57, 73, 45, 5, 51] where a coordinate-based neural network allow to model a continuous field, we propose a novel learnable framework, dubbed Neural Matching Field (NeMF), that aims to establish high-precision correspondence at arbitrary original image resolution. However, typically, matching field between a pair of images is complicated and high-dimensional, where a simple fully-connected network, which is commonly used in INR, may fail to implicitly represent such a high-dimensional matching field. To better structure the intricate matching field, we propose a cost embedding network that takes a coarse cost volume to learn cost feature representation and use it as a guidance for generating high-precision matching field through the following fully-connected network. This is accomplished by designing the cost embedding network with convolutions [18] and self-attention layers [78] to encapsulate local contexts and impart to all pixels with global receptive fields of self-attention, which also helps to compensate for the lack of inductive bias of Transformer by injecting convolutional inductive bias. The intuition of the proposed method is illustrated in Fig. 1(b).

Although leveraging a cost representation may alleviate the issues for learning the matching field with details preserved, naïvely performing feed-forward for all pixels of matching field to find pixel-wise correspondences that are used for providing supervisory signals or inference would be computationally intractable. To this end, we learn a neural matching field by enforcing the network to predict the correctness of a correspondence given a set consisting of randomly sampled points and the ground-truth point. Furthermore, as the intractability issue applies similarly at inference phase, we propose a novel test-time optimization method that not only adopts a PatchMatch [1]-based search space sampling strategy in the learned neural matching, but also optimizes the coordinates for a means of correction that lead to find better correspondences as the iteration progresses. We alternatively perform both PatchMatch-like inference and coordinate optimization, which works as an exploration and exploitation solution.

In the experiments, we evaluate the effectiveness of the proposed method using the standard benchmarks for semantic correspondence [49, 15, 16]. We demonstrate that the proposed implicit matching field effectively finds high precision correspondences, reporting the dramatically boosted performances in comparison to that of hand-crafted interpolation techniques. We also conduct extensive ablation study to validate our design choices and explore the effectiveness of each components.

2 Related Work

Semantic Correspondence. The earliest works [10, 66, 3, 37] focused on feature extraction stage by proposing the hand-crafted feature descriptors. Although these works are probably based on the most well-known traditional hand-crafted feature descriptors, they exhibit limited capability to capture high-level semantics. Resolving such an issue, convolutional neural networks (CNNs) [72, 18] made a paradigm shift thanks to their robust representations to deformations, at first replacing the hand-crafted features with deep features, rapidly converging towards end-to-end learning. Since

(a) Source (b) CATs [8] (c) NeMF (Ours) (d) CATs [8] (e) NeMF (Ours)

Figure 2: **Visualization of matching fields:** (a) source image, where the keypoint is marked as green triangle, (b), (c) 2D contour plots of cost by CATs [8] and the NeMF (ours), respectively, and (d), (e) 3D visualization of cost by CATs [8] and NeMF, with respect to the keypoint in (a). Note that all the visualizations are smoothed by a Gaussian kernel. Compared to CATs [8], NeMF has higher peak near ground-truth and makes a more accurate prediction.

then, leveraging deep features has become the *de facto* standard. Rocco *et al.* [62] first proposed an end-to-end geometric matching networks based on the deep feature maps extracted using CNNs and correlation maps computed between the extracted feature maps. Since then, using correlation map which contains all pairs of similarities between descriptors has become popular by numerous matching networks [65, 63, 43, 76, 19, 31, 48, 50, 47, 64, 26, 34, 82, 32, 40, 8]. However, not only exhaustively computing and storing all pairwise similarities require quadratic memory and computation complexity with respect to the input spatial size, which is a major downside, but also it is infeasible to compute them as the resolution increases. This inevitably caused existing methods to utilize correlation map defined at low resolutions.

On the other hand, notable methods include NC-Net [65] which first proposes to employ 4D convolutions to identify spatially consistent matches by exploring neighbourhood consensus. DHPF [50] applied probabilistic Hough matching (PHM) [7] to find the matching points. CHM [47] extends the PHM by employing high-dimensional convolutional kernels to aggregate 6D correlation maps. CATs [8] and its extension [9] use transformers [78, 12] to explore global consensus from correlation maps thanks to transformers' ability to consider long-range interactions. All these works exploit rich semantics present at high-level features for robust matching across semantically similar images. However, this inevitably necessitates up-sampling the predicted correspondence field to original image-level resolutions, which may result in losing precision. Unlike them, we implicitly represent a matching field at arbitrary image-level resolution, eliminating such a loss and ensure high-precision correspondence field to be found, as shown in Fig. 2.

Implicit Neural Representation. Implicit neural representation (INR), also known as coordinate-based representations, is continuous, differentiable signal representation parameterized by neural networks [45]. INR recently received huge attention, and substantial progress has been made in this direction. INR is not coupled to spatial resolution, making the memory requirements to parameterize the input signals orthogonal to spatial resolution.

Notable contributions to INR include COIN [13] that proposes a compression method with INR and LIIF [5] learns a continuous representation for images that can be presented in arbitrary resolution. DeepSDF [53] was a pioneering work that enables high quality representation from 3D input data by leveraging a learned continuous signed distance function. Occupancy networks [44] implicitly represent the 3D surface as the continuous decision boundary. IM-Net [6] also takes a similar approach, learning a mapping from coordinates conditioned by shape feature vectors to determine whether a point is outside or inside the 3D shape.

Since then, INR-based works consistently have attained state-of-the-art performance in 3D computer vision. As a pioneering work, NeRF [45] represents 3D scenes as neural radiance fields for novel view synthesis. Inspired by NeRF, a large number of works [81, 54, 70, 28, 55, 59, 14, 79, 42, 58, 2, 73, 4, 51, 80, 61, 5] made a progress in this direction. Although flourished in 3D computer vision tasks, INR has never been properly studied or explored in visual correspondence tasks, which we address in this work.

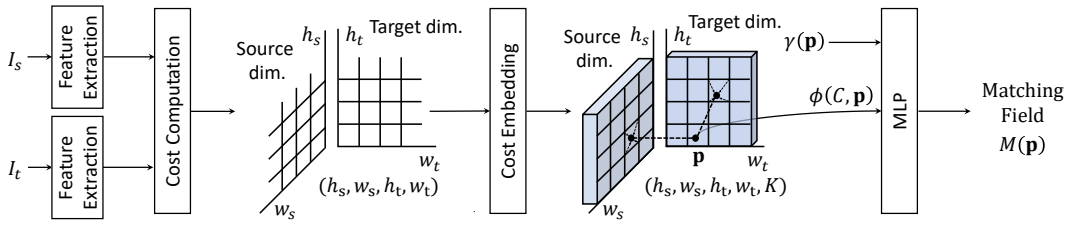

Figure 3: **Overview of network architecture:** Given a pair of images as an input, we first extract features using CNNs [18] and compute an initial noisy cost volume at low resolution. We feed the noisy cost volume with the proposed encoder consisting of convolution [18] and Transformer [78], and decode with deep fully connected networks by taking the encoded cost and coordinates as inputs.

3 Preliminary

Neural Radiance Field (NeRF) is a continuous function f_ω with parameters ω that computes a volume density σ and RGB color value $\mathbf{c} = (r, g, b)$ taking as an input a 3D location $\mathbf{o} = (x, y, z)$ and 2D viewing direction $\mathbf{d} = (\theta, \phi)$, such that $f_\omega : (\mathbf{o}, \mathbf{d}) \rightarrow (\sigma, \mathbf{c})$. In practice, as shown in [45, 74], mapping low dimensional inputs $\mathbf{x}$ and $\mathbf{d}$ to higher dimensional features before passing them through the neural networks enables better representing high frequency variations.

Specifically, denoting $\gamma(\cdot)$ as an encoding function and L as the number of frequency octaves as

$$\gamma(t) = [\sin(2^0 t\pi), \cos(2^0 t\pi), ..., \sin(2^L t\pi), \cos(2^L t\pi)], \tag{1}$$

the overall process $f_\omega : \mathbb{R}^{L_\mathbf{o}} \times \mathbb{R}^{L_\mathbf{d}} \rightarrow \mathbb{R}^+ \times \mathbb{R}^3$ is defined as

$$\{\sigma, \mathbf{c}\} = f_\omega(\gamma(\mathbf{o}), \gamma(\mathbf{d})) \tag{2}$$

where $L_\mathbf{o}$ and $L_\mathbf{d}$ denote output dimension of the encoded coordinate $\mathbf{o}$ and viewing direction $\mathbf{d}$, respectively. The function f_ω is formulated as a fully-connected deep network. This implicit neural representations are not coupled to spatial resolution for using continuous functions, making the memory consumption required to parameterize the signal independent of spatial resolution [45, 74].

4 Neural Matching Fields (NeMF)

4.1 Problem Statement and Overview

The overview of NeMF is shown in Fig. 3. Given a pair of source and target images as $I_s \in \mathbb{R}^{H_s \times W_s}$ and $I_t \in \mathbb{R}^{H_t \times W_t}$, our objective is to find a dense correspondence field $F(\mathbf{x})$ that is defined for each pixel $\mathbf{x}$ in original image resolution, which warps I_s towards I_t so as to satisfy $I_t(\mathbf{x}) \approx I_s(\mathbf{x} + F(\mathbf{x}))$.

Following traditional matching pipeline, we first extract dense features D_s and D_t from the input source and target images, and then compute full pair-wise similarity scores between them using cosine distance such that:

$$C(\mathbf{x}, \mathbf{y}) = \frac{D_s(\mathbf{x}) \cdot D_t(\mathbf{y})}{\|D_s(\mathbf{x})\| \|D_t(\mathbf{y})\|}, \tag{3}$$

where $\mathbf{x} \in [0, h_s) \times [0, w_s)$ and $\mathbf{y} \in [0, h_t) \times [0, w_t)$, and $\| \cdot \|$ denotes l-2 normalization. Previous approaches [50, 47, 8] extracted features from the deep layers of CNN to have high-level semantic invariance, resulting the spatial resolution of D_s and D_t to be reduced, i.e., $h < H$ and $w < W$. Consequently, utilizing the coarse similarity scores $C(\mathbf{x}, \mathbf{y})$ to infer correspondences inevitably yields a low-resolution correspondence map, which additionally requires post-processing to be interpolated into a high-resolution map [8, 47].

To alleviate this issue, we propose an INR-based learnable framework, called neural matching field (NeMF), that implicitly represents a high-dimensional 4D matching field to infer high-precision correspondences at arbitrary scales without any post-processing procedure. Specifically, we formulate a continuous function f_θ as a multi layer perceptron (MLP) with parameters θ in which encoded position and its corresponding cost feature vector are taken as an input. Formally, denoting 4D coordinates defined in original image resolution as $\mathbf{p} = [\mathbf{x}, \mathbf{y}]$ where $\mathbf{x} \in [0, H_s) \times [0, W_s)$ and $\mathbf{y} \in [0, H_t) \times [0, W_t)$, our neural matching field $M \in \mathbb{R}^{H_s \times W_s \times H_t \times W_t}$ is computed as

$$M(\mathbf{p}) = f_\theta(\gamma(\mathbf{p}), \phi(C, \mathbf{p})) \in [0, 1], \tag{4}$$

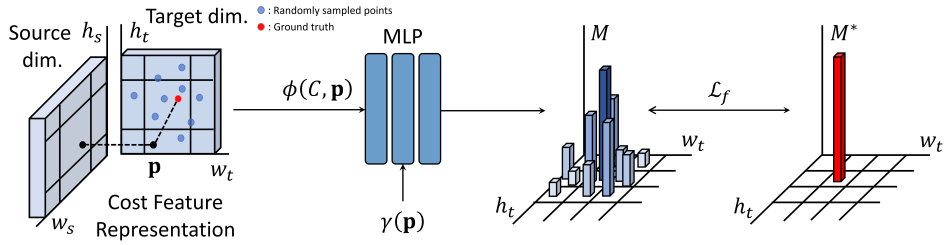

Figure 4: **Overview of neural matching field optimization:** Given an encoded cost, we randomly sample coordinates from uniform distribution. The random coordinates and ground-truth coordinate are then processed altogether to obtain the matching scores and the cross-entropy loss is computed for the training signal.

where $\gamma(\mathbf{p})$ is an encoded point of $\mathbf{p}$, and $\phi(C, \mathbf{p})$ denotes the cost feature vector at $\mathbf{p}$ extracted from coarse cost volume C. A possible way for the architecture design of function f_θ is first concatenating the two inputs $\gamma(\mathbf{p})$ and $\phi(C, \mathbf{p})$, and then passing them through the fully-connected network. This approach, however, may impose memory intensive batch normalization operation [44]. To address this, we adopt the architecture of [52], where $\phi(C, \mathbf{p})$ is added to the input features of each fully-connected block. In addition, to guarantee the value of 4D matching cost fields to be lied within the range from 0 to 1, we use a sigmoid function [17] at the end of the networks.

4.2 Cost Embedding Network

Our assumption is that formulating the function $f_\theta(\cdot)$ without any condition may be challenged when representing complicated and high-dimensional continuous field. We address this by introducing cost embedding network where the raw cost volume is further embedded into a cost feature volume $\phi(C, \mathbf{p})$, which is used as a guidance for establishing high-precision matching field through the following fully-connected network $f_\theta(\cdot)$.

Motivated by recent works [8, 22] that aggregate matching costs for better correspondence hypothesis, we further embed the raw cost volume through the global receptive fields of self-attention layer [78, 12]. Although these representations are explicitly encoded from all pixels of a cost volume, the absence of operations that impart inductive bias, *i.e.,* translation equivariance by convolutions or relative positioning bias, may yield representations with errors. To this end, we combine Transformer architecture [78] with convolution operator to compensate the lack of inductive bias, allowing local and global integration of matching cues by encapsulating the local contexts and imparting them to all pixels via self-attention. Concretely, before providing matching cost to the function f_θ, the 4D raw cost volume C is embedded into 5D cost feature volume $C' \in \mathbb{R}^{H_s \times W_s \times H_t \times W_t \times K}$ with K channels which is still defined at low resolution. We then use a quadlinear interpolation on C' for a query point $\mathbf{p}$ to a cost feature vector $\phi(C, \mathbf{p}) \in \mathbb{R}^{K \times 1}$.

4.3 Training

As shown in Fig. 4, to train the networks, we use a ground-truth keypoint pair $\{\mathbf{x}, \mathbf{x}'\}$ between an input image pair in a manner that if a query point $\mathbf{p} = [\mathbf{x}, \mathbf{y}]$ is classified as the ground-truth correspondence, *i.e.,* $\mathbf{y} = \mathbf{x}'$, the network output should be encouraged to be 1, and 0 otherwise. We formulate this as a classification problem, and thus we apply cross-entropy loss to learn to predict the correctness of a correspondence for a query $\mathbf{x}$ in the source image among sampled negative keypoints $\mathbf{y}$ in the target image (where $\mathbf{y} \neq \mathbf{x}'$) and that of ground-truth $\mathbf{x}'$. Even though the better negative sampling techniques, e.g., hard negative mining [27, 24], can be used, in experiments, we simply adopt random sampling from uniform distribution as negative samples, as background clutters or extreme geometric variations inherently present across semantic correspondence datasets [15, 16, 49] would contribute to robust representation learning. Formally, the loss function is defined as follows:

$$\mathcal{L}_f = -\sum_{k=1}^{K} M_k^* \log(M(\mathbf{p}_k)), \tag{5}$$

where $\mathbf{p}_k$ denotes k-th query samples for $k \in \{1, ..., K\}$, and M_k^* is a ground-truth matching score, e.g., $M_k^* = 1$ if $\mathbf{p}_k$ is a ground-truth keypoint pair, and 0 otherwise.

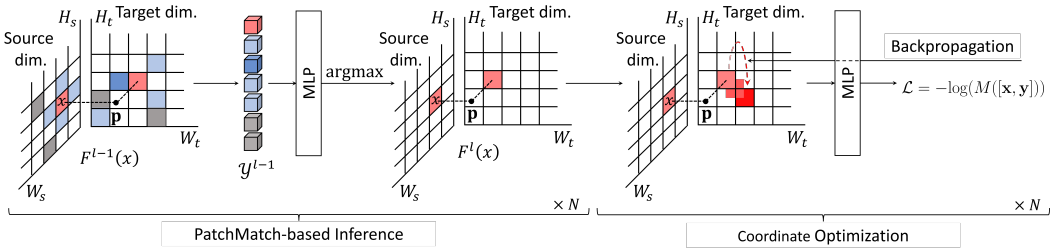

Figure 5: **Illustration of the proposed PatchMatch and coordinate optimization:** With the learned neural matching field, the proposed PatchMatch injects explicit smoothness and reduces the search range. The subsequent optimization strategy searches for a location that maximizes the score of MLP.

Although this would provide sufficient supervisory signal, we found it is beneficial to provide an additional explicit supervisory signal for learning better cost features, which positively affect our PatchMatch [1]-based inference strategy as will be further detailed in Sec. 4.4. To this end, we use end-point-error [8] between the predicted keypoints using the cost feature representations $\phi(C, \mathbf{p})$ directly and the ground-truth keypoints. Concretely, we obtain a channel-wise average pooled cost feature volume $V = \text{avgpool}(\phi(C, \mathbf{p})) \in \mathbb{R}^{H_s \times W_s \times H_t \times W_t}$ and compute F_{pred} by applying soft argmax function to V. We then calculate the Euclidean distance between the ground-truth flow map computed using the ground-truth keypoints and the predicted flow map as

$$\mathcal{L}_c = \|F_{\text{gt}} - F_{\text{pred}}\|_2. \tag{6}$$

Combining with Eq. 6, we define the final objective function $\mathcal{L}_{\text{total}}$ with balancing weights λ_f and λ_c: $\mathcal{L}_{\text{total}} = \lambda_f \mathcal{L}_f + \lambda_c \mathcal{L}_c$.

4.4 Inference

PatchMatch-based Sampling. At the inference stage, we aim to find a dense correspondence field $F(\mathbf{x})$ by leveraging the trained network to determine the correct correspondence for each query $\mathbf{p} = [\mathbf{x}, \mathbf{y}]$. However, searching the best match for each coordinate $\mathbf{x}$ over all possible matching candidates $\mathbf{y}$ in exhaustive manner results in $H_s \times W_s \times H_t \times W_t$ number of feed-forward per sample, which is an extremely time consuming and computationally intensive.

To alleviate the issue, we propose PatchMatch [1]-based sampling. PatchMatch [1] runs a sequence of propagation and update steps to reduce a search space. We use the learned NeMF f_θ as a scoring function to determine the correspondence. To overcome its time-consuming process induced by serial processing inherited from PatchMatch [1], we propose a GPU-friendly PatchMatch optimization that performs propagation and update in a parallel manner.

Specifically, for initialization, we utilize an average pooled cost feature volume V introduced in Section 4.3 . Note that the objective of Eq. 6 directly connects to the initialization step of this approach. This implies that the better cost feature representations would help to obtain a better initialization for PatchMatch-based inference. Then for a query $\mathbf{x}$, we sample a set of candidate correspondences by considering adjacent pixels such that $\mathcal{Z}^{l-1} = \{F^{l-1}(\mathbf{z})\}_{\mathbf{z}}$ for adjacent pixels $\mathbf{z}$ at $(l-1)$-th iteration. In addition, a few random points sampled from a uniform distribution are used to augment $\mathcal{Z}^{l-1}$ such that $\mathcal{Y}^{l-1} = \bigcup \left(\mathcal{Z}^{l-1}, \{\mathbf{y}\}\right)$ for randomly sampled pixels $\mathbf{y}$ where $\bigcup$ denotes an union of the sets. Then the correspondence fields are undated by considering the set of matching candidate $\mathcal{Y}^{l-1}$ such that

$$F^l(\mathbf{x}) = \text{argmax}_{\mathbf{y} \in \mathcal{Y}^{l-1}}(M([\mathbf{x}, \mathbf{y}])). \tag{7}$$

This process is iterated until the convergence. In practice, this candidate selection and scoring run in parallel for every target pixel. This makes the inference process efficient and GPU-friendly in the original resolution, compared to serial propagation and update in [30].

Coordinate Optimization. Although the proposed PatchMatch-based inference strategy could prevent exhaustive searching by effectively sampling the search range for determining the correct correspondence for each pixel, this may degrade the performance due to several reasons including insufficient number of iterations that may result in a sub-optimal solution and a limited search range that provides relatively fewer candidates for consideration. To address this issue, we provide a means

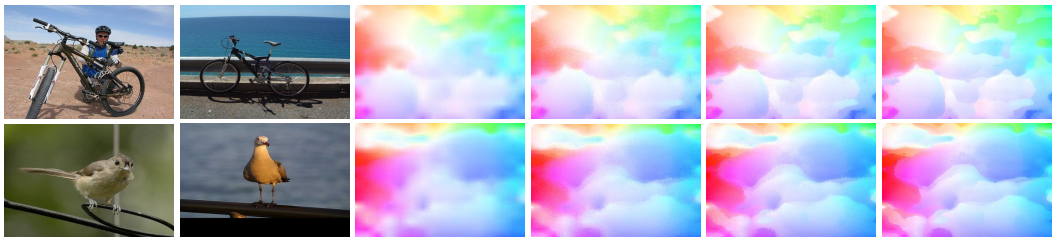

(a) Source (b) Target (c) N = 5 (d) N = 10 (e) N = 15 (f) N = 20

Figure 6: **Visualization of flow maps for different N iterations:** (a) source image, (b) target image. As the number of iteration we set increases along (c), (d), (e) and (f) at inference phase, NeMF with trained MLP predicts more precise matching fields by PatchMatch-based sampling and coordinate optimization. Note that different colors of flow maps indicate directions and magnitudes of the flows.

to reduce the potential erroneous inference by adopting test-time optimization strategy that directly optimize coordinates $\mathbf{y}$ that maximizes the correctness of the correspondence using the learned the network f_θ.

Concretely, because the network f_θ is naturally differentiable, as shown in Fig. 5, we use a gradient descent to optimize the target coordinate $\mathbf{y}$ in the direction of decreasing the negative log likelihood of the matching score, with respect to the corresponding source coordinate $\mathbf{x}$. Formally, the coordinate optimization is performed by iterative updates which can be formulated as:

$$\begin{aligned} \mathcal{L} &= -\log(M([\mathbf{x}, \mathbf{y}])), \\ \mathbf{y} &:= \mathbf{y} - \alpha \nabla_{\mathbf{y}} \mathcal{L}, \end{aligned} \tag{8}$$

where α denotes a step size. Any advanced optimizer can also be used for improved optimization [60, 39]. Note that the source coordinate is not updated during this optimization. With the proposed coordinate optimization, we combine with PatchMatch-based sampling to establish a final correspondence field as shown in Fig. 5. Each iteration number is defined as N. As exemplified in Fig. 6, NeMF predicts more precise matching fields by PatchMatch-based sampling and coordinate optimization as evolving iterations.

Note that the key difference of this test-time optimization to that of DMP [19] is that we optimize the coordinates to correct themselves to find a better correspondence with by leveraging the already learned network, while DMP optimizes the parameters of the networks.

5 Experiments

5.1 Implementation Details

For backbone feature extractor, we use ResNet-101 [18] pre-trained on ImageNet [11]. We use the feature maps resized to 16×16 for constructing a coarse cost volume. For the cost embedding network, we build upon [8] and its implementations. We implemented our network using PyTorch [56], and AdamW [41] optimizer with an initial learning rate of 3e−5. We set N = 10 for both PatchMatch and coordinate optimizations, and learning rate of 3e−4 is used for coordinate optimization. Additional details are provided in the supplemenatry material.

5.2 Experimental Settings

Datasets. We use three benchmarks, which include SPair-71k [49], PF-PASCAL [16] and PF-WILLOW [15], to evaluate the effectiveness of the proposed method. SPair-71k [49] provides total 70,958 image pairs, PF-PASCAL [16] contains 1,351 image pairs from 20 categories, and PF-WILLOW [15] contains 900 image pairs from 4 categories. Each dataset contains ground-truth annotations, which we use them for evaluation and training.

Evaluation Metric. For the evaluation metric, we employ a percentage of correct keypoints (PCK), which is computed as the ratio of estimated keypoints within the threshold from ground-truths to the total number of keypoints. Assume a predicted keypoint k_{pred} and a ground-truth keypoint k_{GT}, the number of correctly predicted keypoints are counted, and the condition for deciding the

Table 1: **Quantitative evaluation on standard benchmarks [49, 15, 16, 75]:** Higher PCK is better. The best results are in bold, and the second best results are underlined. All results are taken from the papers. *Eval. Reso.: Evaluation Resolution, Flow Reso.: Flow Resolution.*

Methods	Eval. Reso.	Flow Reso.	SPair-71k [49] PCK @ α_{bbox}				PF-PASCAL [16] PCK @ α_{img}				PF-WILLOW [15] PCK @ $\alpha_{\text{bbox-kp}}$			
			0.01	0.03	0.05	0.1	0.01	0.03	0.05	0.1	0.01	0.03	0.05	0.1
CNNGeo [62]	ori	-	-	-	-	20.6	-	-	41.0	69.5	-	-	36.9	69.2
A2Net [71]	-	-	-	-	-	22.3	-	-	42.8	70.8	-	-	36.3	68.8
WeakAlign [63]	ori	-	-	-	-	20.9	-	-	49.0	74.8	-	-	37.0	70.2
RTNs [29]	-	-	-	-	-	25.7	-	-	55.2	75.9	-	-	41.3	71.9
SFNet [32]	288/ori	20	-	-	-	-	-	-	53.6	81.9	-	-	46.3	74.0
PARN [25]	-	-	-	-	-	-	-	-	26.8	49.1	-	-	-	-
PMD [35]	-	20	-	-	-	37.4	-	-	-	90.7	-	-	-	75.6
PMNC [31]	400	-	-	-	-	50.4	-	-	**82.4**	90.6	-	-	-	-
MMNet [82]	224×320	-	-	-	-	40.9	-	-	77.6	89.1	-	-	-	-
DCC-Net [21]	240/ori/-	-	-	-	-	-	-	-	55.6	82.3	-	-	43.6	73.8
HPF [48]	max 300	-	-	-	-	28.2	-	-	60.1	84.8	-	-	45.9	74.4
GSF [26]	-	-	-	-	-	36.1	-	-	65.6	87.8	-	-	49.1	**78.7**
ANC-Net [34]	240	15	-	-	-	-	-	-	-	86.1	-	-	-	-
NC-Net [65]	240/ori/-	15	-	-	-	20.1	-	-	54.3	78.9	-	-	33.8	67.0
DHPF [50]	240	15	-	-	-	37.3	-	-	75.7	90.7	-	-	-	71.0
CHM [47]	240	15	-	-	-	46.3	-	-	80.1	91.6	-	-	-	69.6
CATs [8]	256	16	2.3	13.8	27.7	49.9	7.7	49.9	75.4	92.6	2.9	20.4	40.7	69.0
NeMF	ori	ori	**3.2**	**19.5**	**34.2**	**53.6**	**18.6**	**61.6**	80.6	**93.6**	**3.8**	**25.4**	**60.8**	75.0

Table 2: **Per-class quantitative evaluation on SPair-71k [49] benchmark.**

Methods	aero.	bike	bird	boat	bott.	bus	car	cat	chai.	cow	dog	hors.	mbik.	pers.	plan.	shee.	trai.	tv	all
CNNGeo [62]	23.4	16.7	40.2	14.3	36.4	27.7	26.0	32.7	12.7	27.4	22.8	13.7	20.9	21.0	17.5	10.2	30.8	34.1	20.6
WeakAlign [63]	22.2	17.6	41.9	15.1	38.1	27.4	27.2	31.8	12.8	26.8	22.6	14.2	20.0	22.2	17.9	10.4	32.2	35.1	20.9
NC-Net [65]	17.9	12.2	32.1	11.7	29.0	19.9	16.1	39.2	9.9	23.9	18.8	15.7	17.4	15.9	14.8	9.6	24.2	31.1	20.1
HPF [48]	25.2	18.9	52.1	15.7	38.0	22.8	19.1	52.9	17.9	33.0	32.8	20.6	24.4	27.9	21.1	15.9	31.5	35.6	28.2
SCOT [40]	34.9	20.7	63.8	21.1	43.5	27.3	21.3	63.1	20.0	42.9	42.5	31.1	29.8	35.0	27.7	24.4	48.4	40.8	35.6
DHPF [50]	38.4	23.8	68.3	18.9	42.6	27.9	20.1	61.6	22.0	46.9	46.1	33.5	27.6	40.1	27.6	28.1	49.5	46.5	37.3
CHM [47]	49.1	33.6	64.5	32.7	44.6	47.5	43.5	57.8	21.0	61.3	54.6	43.8	35.1	43.7	38.1	33.5	70.6	55.9	46.3
MMNet [82]	43.5	27.0	62.4	27.3	40.1	50.1	37.5	60.0	21.0	56.3	50.3	41.3	30.9	19.2	30.1	33.2	64.2	43.6	40.9
PMNC [30]	54.1	35.9	74.9	36.5	42.1	48.8	40.0	**72.6**	21.1	**67.6**	58.1	50.5	40.1	**54.1**	**43.3**	35.7	74.5	59.9	50.4
CATs [8]	52.0	34.7	72.2	34.3	49.9	57.5	43.6	66.5	24.4	63.2	56.5	52.0	42.6	41.7	43.0	33.6	72.6	58.0	49.9
NeMF	**55.6**	**37.2**	**76.2**	**36.9**	**54.1**	**62.1**	**47.5**	70.5	**26.2**	**67.6**	**59.3**	**57.1**	**48.0**	40.2	42.1	**36.7**	**80.7**	**66.1**	**53.6**

correctness is defined as follows: $d(k_{\text{pred}}, k_{\text{GT}}) \leq \alpha \cdot \max(H, W)$, where $d(\cdot)$ and α denote Euclidean distance and a threshold. When we evaluate on PF-PASCAL, we use α_{img} following other works [16, 48, 50, 8], SPair-71k and PF-WILLOW with α_{bbox}; H and W denote height and width of the object bounding box or entire image, respectively.

5.3 Matching Results

To ensure a fair comparison, the model evaluated on SPair-71k [49] is trained on training split of SPair-71k [49] and the model evaluated on PF-PASCAL [16] and PF-WILLOW [15] is trained on training split of PF-PASCAL [16].

The results are summarized in Table 1 and the qualitative results are shown in Fig. 7. We note the resolution which the method is evaluated, since [9, 77] observe that the resolution of images affect the PCK performance, and the resolution of which the method outputs the correspondence field. It is shown that NeMF achieves competitive performance or even attains state-of-the-art performance for several alpha thresholds. More concretely, for lower alpha thresholds, we tend to achieve higher PCK compared to other works. This implies that the existing works, which rely on interpolation techniques that prevent from fine-grained matching due to the use of matching field defined at low resolution, may have suffered from the large resolution gap between the predicted flow and that of ground-truth. For example, CATs [8] processes the cost volume at 16^4 and infers a flow map at this resolution. On the contrary, NeMF avoids this by implicitly representing a matching field at higher resolution, demonstrating its advantageous approach.

5.4 Ablation Study

In this section, we conduct ablation study to investigate the effectiveness of different configurations for cost embedding network and effectiveness of the proposed inference strategies. We train the networks on the training split of SPair-71k [49] and evaluated on the test split.

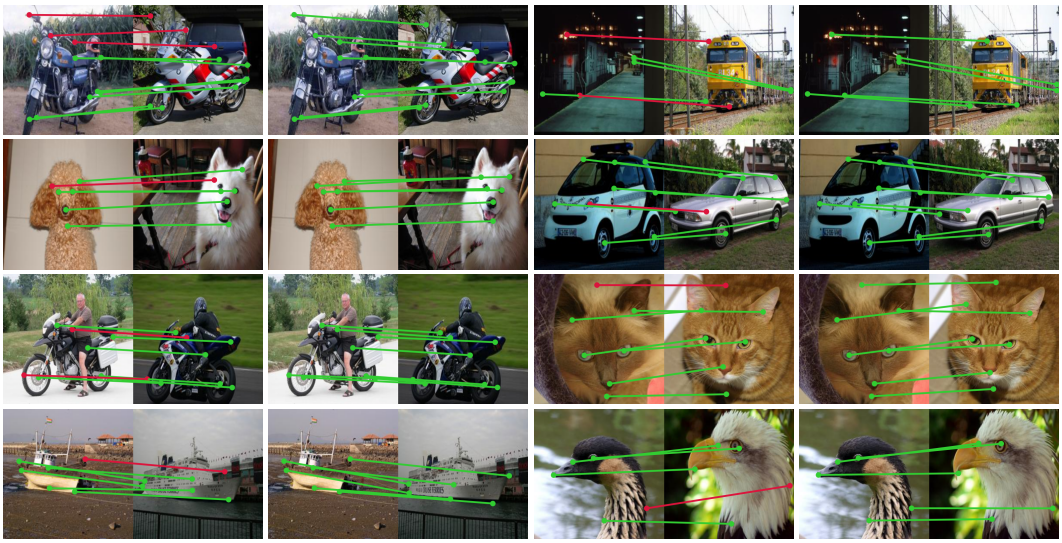

(a) CATs [8] (b) NeMF (c) CATs [8] (d) NeMF

Figure 7: **Qualitative results on PF-PASCAL [16]:** keypoint transfer results by (a), (c) CATs [8] and (b), (d) NeMF. Green and red line denote correct and wrong prediction ($\alpha_{\text{img}} = 0.1$), respectively. Note that correspondences are estimated at the original resolutions of iamges.

Different Cost Feature Representation. Table 3 summarizes the comparison between the effectiveness of cost feature representations learned from different configurations of cost embedding network. In this ablation study, we compare four configurations. (**I**) shows the results for exploiting raw cost volume defined at coarse level. From (**II**) to (**IV**), we show the effectiveness of extracting cost features via convolutions, self-attention layers and integration of both, respectively.

We observe that simply leveraging a raw cost volume struggles to learn a complicated matching field, as it does not provide a sufficient structural or detailed information among pixel-wise similarities. As the cost embedding network is introduced to learn feature representations, the performance is dramatically boosted, and our approach clearly helps to attain the best performance by learning more powerful representations than (**II**) and (**III**).

Table 3: **Cost feature representation.**

	Components	SPair-71k [49] PCK @ α_{bbox}				
		0.01	0.03	0.05	0.1	0.15
(I)	Coarse cost volume	0.3	2.3	5.8	15.5	25.7
(II)	Conv.	2.2	14.6	28.3	48.9	59.4
(III)	Self-attention	2.5	16.4	30.6	51.7	61.7
(IV)	Conv. + self-attention	3.2	19.5	34.2	53.6	63.3

Inference Strategies. In this ablation study, we aim to show a quantitative comparison between different strategies at the inference phase. Table 4 summarizes the results. Note that we included (**I**) to highlight that at the inference phase, the evaluation on a pair of images with original resolution, for example, would take approximately more than 300k seconds. This clearly shows the infeasibility of adopting naïve inference strategy.

Table 4: **Inference strategy.** *TL* denotes Too Long.

	Components	SPair-71k [49] PCK @ α_{bbox}					Average run-time per sample [s]
		0.01	0.03	0.05	0.1	0.15	
(I)	Exhaustive infer.	*TL*	*TL*	*TL*	*TL*	*TL*	> 300k
(II)	PatchMatch-based infer.	1.1	7.7	15.3	31.4	41.9	7.75
(III)	(**II**) + coordinate opt.	3.2	19.5	34.2	53.6	63.3	8.20

From (**II**) to (**III**), we observe an apparent performance boost, which demonstrates that the proposed test-time coordinate optimization helps to correct the coordinates for finding better correspondences. However, this approach has a downside. Applying coordinate optimization inevitably increases the time taken for the inference, which is a typical limitation of test-time optimization. However, 0.5 second is a minor sacrifice for a better performance. Note that further improvement could be made by adopting better optimizing strategy, *i.e.,* learning rate, search range or optimizer.

Computational Complexity. Although the proposed inference strategy enables significantly reduced time for establishing correspondence field between a pair of images, in practice, we observe that assuming we set $N = 10$, the time taken at the inference phase for a single sample is approximately 8-9 seconds on a single GPU Geforce RTX 3090, which prevents from a real-time inference. This is an apparent limitation of the proposed approach, but we refer the readers to supplementary material where we show that without affecting the performance, the memory consumption and run-time can be controlled.

In addition, we also provide experimental results that demonstrates the efficiency of the proposed approach in comparison to existing works, which is summarized in Table 5. Let us assume that we are representing cost volumes of four different resolutions, *e.g.,* 16, 32, 64 and 128. At the training phase, unlike other works that inevitably consume more memory as the resolution increases, the proposed approach successfully deviates from it thanks to the proposed training strategy. Furthermore, at the inference phase, we observe that the proposed approach has an advantage over other methods. Although NeMF may suffer from relatively larger computation and memory consumption than CATs [8] and CHM [47] when the resolution is low, it has an advantage when the resolution is high, allowing the network to exploit highly accurate cost volume with relatively less memory consumption.

Table 5: **Memory Comparison.** [MiB] *OOM : Out of Memory*

Method	Train	Inference	16^4	32^4	64^4	128^4
CHM [47]	✓	✗	708	1,538	OOM	OOM
	✗	✓	371	433	OOM	OOM
CATs [8]	✓	✗	454	3,523	OOM	OOM
	✗	✓	188	302	1882	OOM
NeMF	✓	✗	4,205	4,205	4,205	4,205
	✗	✓	1,528	1,528	2,443	6,309

6 Conclusion

In this paper, we proposed a novel INR-based architecture, called neural matching fields (NeMF), that implicitly represent a 4D matching field to find high-precision correspondences. This method proposed an architecture and training and inference procedures targeted to handle complicacy and high-dimensionality of a matching field that acts as major hindrances. Specifically, we embed the raw cost volume with convolutions and Transformer to obtain local and global integration of matching cues to handle the complicacy, and sampling-based training and inference procedure to handle the high-dimensionality. We have shown that the proposed method attains state-of-the-art performance on several benchmarks for semantic correspondence. We also conducted an extensive ablation study to validate our choices.

Broader Impact

Our implicit representation of cost volume may be beneficial for other domains that utilize a correlation map, which include semantic segmentation [67, 75, 46], object detection [36], and image editing [37]. It can help to boost the performance by preserving the fine-detailed information within the cost volume. However, as the proposed approach aims to implicitly represent the cost volume, on its own, it is not feasible to use for a malicious purpose.

Acknowledgements. This research was supported by the MSIT, Korea (IITP-2022-2020-0-01819, ICT Creative Consilience program, No. 2020-0-00368, A Neural-Symbolic Model for Knowledge Acquisition and Inference Techniques), and National Research Foundation of Korea (NRF-2021R1C1C1006897).

References

[1] Connelly Barnes, Eli Shechtman, Adam Finkelstein, and Dan B Goldman. Patchmatch: A randomized correspondence algorithm for structural image editing. *ACM Trans. Graph.*, 28(3):24, 2009.

[2] Jonathan T Barron, Ben Mildenhall, Matthew Tancik, Peter Hedman, Ricardo Martin-Brualla, and Pratul P Srinivasan. Mip-nerf: A multiscale representation for anti-aliasing neural radiance fields. In *Proceedings of the IEEE/CVF International Conference on Computer Vision*, pages 5855–5864, 2021.

[3] Herbert Bay, Tinne Tuytelaars, and Luc Van Gool. Surf: Speeded up robust features. In *European conference on computer vision*, pages 404–417. Springer, 2006.

[4] Eric R Chan, Marco Monteiro, Petr Kellnhofer, Jiajun Wu, and Gordon Wetzstein. pi-gan: Periodic implicit generative adversarial networks for 3d-aware image synthesis. In *Proceedings of the IEEE/CVF conference on computer vision and pattern recognition*, pages 5799–5809, 2021.

[5] Yinbo Chen, Sifei Liu, and Xiaolong Wang. Learning continuous image representation with local implicit image function. In *Proceedings of the IEEE/CVF Conference on Computer Vision and Pattern Recognition*, pages 8628–8638, 2021.

[6] Zhiqin Chen and Hao Zhang. Learning implicit fields for generative shape modeling. In *Proceedings of the IEEE/CVF Conference on Computer Vision and Pattern Recognition*, pages 5939–5948, 2019.

[7] Minsu Cho, Suha Kwak, Cordelia Schmid, and Jean Ponce. Unsupervised object discovery and localization in the wild: Part-based matching with bottom-up region proposals. In *Proceedings of the IEEE conference on computer vision and pattern recognition*, pages 1201–1210, 2015.

[8] Seokju Cho, Sunghwan Hong, Sangryul Jeon, Yunsung Lee, Kwanghoon Sohn, and Seungryong Kim. Cats: Cost aggregation transformers for visual correspondence. In *Thirty-Fifth Conference on Neural Information Processing Systems*, 2021.

[9] Seokju Cho, Sunghwan Hong, and Seungryong Kim. Cats++: Boosting cost aggregation with convolutions and transformers. *arXiv preprint arXiv:2202.06817*, 2022.

[10] Navneet Dalal and Bill Triggs. Histograms of oriented gradients for human detection. In *CVPR Workshops)*, 2005.

[11] Jia Deng, Wei Dong, Richard Socher, Li-Jia Li, Kai Li, and Li Fei-Fei. Imagenet: A large-scale hierarchical image database. In *2009 IEEE conference on computer vision and pattern recognition*. Ieee, 2009.

[12] Alexey Dosovitskiy, Lucas Beyer, Alexander Kolesnikov, Dirk Weissenborn, Xiaohua Zhai, Thomas Unterthiner, Mostafa Dehghani, Matthias Minderer, Georg Heigold, Sylvain Gelly, et al. An image is worth 16x16 words: Transformers for image recognition at scale. *arXiv preprint arXiv:2010.11929*, 2020.

[13] Emilien Dupont, Adam Goliński, Milad Alizadeh, Yee Whye Teh, and Arnaud Doucet. Coin: Compression with implicit neural representations. *arXiv preprint arXiv:2103.03123*, 2021.

[14] Guy Gafni, Justus Thies, Michael Zollhofer, and Matthias Nießner. Dynamic neural radiance fields for monocular 4d facial avatar reconstruction. In *Proceedings of the IEEE/CVF Conference on Computer Vision and Pattern Recognition*, pages 8649–8658, 2021.

[15] Bumsub Ham, Minsu Cho, Cordelia Schmid, and Jean Ponce. Proposal flow. In *CVPR*, 2016.

[16] Bumsub Ham, Minsu Cho, Cordelia Schmid, and Jean Ponce. Proposal flow: Semantic correspondences from object proposals. *IEEE transactions on pattern analysis and machine intelligence*, 2017.

[17] Jun Han and Claudio Moraga. The influence of the sigmoid function parameters on the speed of back-propagation learning. In *International workshop on artificial neural networks*, pages 195–201. Springer, 1995.

[18] Kaiming He, Xiangyu Zhang, Shaoqing Ren, and Jian Sun. Deep residual learning for image recognition. In *Proceedings of the IEEE conference on computer vision and pattern recognition*, 2016.

[19] Sunghwan Hong and Seungryong Kim. Deep matching prior: Test-time optimization for dense correspondence. In *Proceedings of the IEEE/CVF International Conference on Computer Vision (ICCV)*, 2021.

[20] Asmaa Hosni, Christoph Rhemann, Michael Bleyer, Carsten Rother, and Margrit Gelautz. Fast cost-volume filtering for visual correspondence and beyond. *PAMI*, 2012.

[21] Shuaiyi Huang, Qiuyue Wang, Songyang Zhang, Shipeng Yan, and Xuming He. Dynamic context correspondence network for semantic alignment. In *ICCV*, 2019.

[22] Zhaoyang Huang, Xiaoyu Shi, Chao Zhang, Qiang Wang, Ka Chun Cheung, Hongwei Qin, Jifeng Dai, and Hongsheng Li. Flowformer: A transformer architecture for optical flow. *arXiv preprint arXiv:2203.16194*, 2022.

[23] Eddy Ilg, Nikolaus Mayer, Tonmoy Saikia, Margret Keuper, Alexey Dosovitskiy, and Thomas Brox. Flownet 2.0: Evolution of optical flow estimation with deep networks. In *CVPR*, 2017.

[24] Allan Jabri, Andrew Owens, and Alexei Efros. Space-time correspondence as a contrastive random walk. *Advances in neural information processing systems*, 33:19545–19560, 2020.

[25] Sangryul Jeon, Seungryong Kim, Dongbo Min, and Kwanghoon Sohn. Parn: Pyramidal affine regression networks for dense semantic correspondence. In *Proceedings of the European Conference on Computer Vision (ECCV)*, pages 351–366, 2018.

[26] Sangryul Jeon, Dongbo Min, Seungryong Kim, Jihwan Choe, and Kwanghoon Sohn. Guided semantic flow. In *ECCV*. Springer, 2020.

[27] Sangryul Jeon, Dongbo Min, Seungryong Kim, and Kwanghoon Sohn. Mining better samples for contrastive learning of temporal correspondence. In *Proceedings of the IEEE/CVF Conference on Computer Vision and Pattern Recognition*, pages 1034–1044, 2021.

[28] Yoonwoo Jeong, Seokjun Ahn, Christopher Choy, Anima Anandkumar, Minsu Cho, and Jaesik Park. Self-calibrating neural radiance fields. In *Proceedings of the IEEE/CVF International Conference on Computer Vision*, pages 5846–5854, 2021.

[29] Seungryong Kim, Stephen Lin, Sang Ryul Jeon, Dongbo Min, and Kwanghoon Sohn. Recurrent transformer networks for semantic correspondence. *Advances in neural information processing systems*, 31, 2018.

[30] Jae Yong Lee, Joseph DeGol, Victor Fragoso, and Sudipta N. Sinha. Patchmatch-based neighborhood consensus for semantic correspondence. In *Proceedings of the IEEE/CVF Conference on Computer Vision and Pattern Recognition (CVPR)*.

[31] Jae Yong Lee, Joseph DeGol, Victor Fragoso, and Sudipta N Sinha. Patchmatch-based neighborhood consensus for semantic correspondence. In *Proceedings of the IEEE/CVF Conference on Computer Vision and Pattern Recognition*, pages 13153–13163, 2021.

[32] Junghyup Lee, Dohyung Kim, Jean Ponce, and Bumsub Ham. Sfnet: Learning object-aware semantic correspondence. In *CVPR*, 2019.

[33] Jesse Levinson, Jake Askeland, Jan Becker, Jennifer Dolson, David Held, Soeren Kammel, J Zico Kolter, Dirk Langer, Oliver Pink, Vaughan Pratt, et al. Towards fully autonomous driving: Systems and algorithms. In *2011 IEEE intelligent vehicles symposium (IV)*, pages 163–168. IEEE, 2011.

[34] Shuda Li, Kai Han, Theo W Costain, Henry Howard-Jenkins, and Victor Prisacariu. Correspondence networks with adaptive neighbourhood consensus. In *Proceedings of the IEEE/CVF Conference on Computer Vision and Pattern Recognition*, pages 10196–10205, 2020.

[35] Xin Li, Deng-Ping Fan, Fan Yang, Ao Luo, Hong Cheng, and Zicheng Liu. Probabilistic model distillation for semantic correspondence. In *Proceedings of the IEEE/CVF Conference on Computer Vision and Pattern Recognition*, pages 7505–7514, 2021.

[36] Tsung-Yi Lin, Piotr Dollár, Ross Girshick, Kaiming He, Bharath Hariharan, and Serge Belongie. Feature pyramid networks for object detection. In *CVPR*, 2017.

[37] Ce Liu, Jenny Yuen, and Antonio Torralba. Sift flow: Dense correspondence across scenes and its applications. *IEEE transactions on pattern analysis and machine intelligence*, 33(5):978–994, 2010.

[38] Liu Liu, Hongdong Li, and Yuchao Dai. Efficient global 2d-3d matching for camera localization in a large-scale 3d map. In *Proceedings of the IEEE International Conference on Computer Vision*, pages 2372–2381, 2017.

[39] Liyuan Liu, Haoming Jiang, Pengcheng He, Weizhu Chen, Xiaodong Liu, Jianfeng Gao, and Jiawei Han. On the variance of the adaptive learning rate and beyond. *arXiv preprint arXiv:1908.03265*, 2019.

[40] Yanbin Liu, Linchao Zhu, Makoto Yamada, and Yi Yang. Semantic correspondence as an optimal transport problem. In *Proceedings of the IEEE/CVF Conference on Computer Vision and Pattern Recognition*, 2020.

[41] Ilya Loshchilov and Frank Hutter. Decoupled weight decay regularization. *arXiv preprint arXiv:1711.05101*, 2017.

[42] Ricardo Martin-Brualla, Noha Radwan, Mehdi SM Sajjadi, Jonathan T Barron, Alexey Dosovitskiy, and Daniel Duckworth. Nerf in the wild: Neural radiance fields for unconstrained photo collections. In *Proceedings of the IEEE/CVF Conference on Computer Vision and Pattern Recognition*, pages 7210–7219, 2021.

[43] Iaroslav Melekhov, Aleksei Tiulpin, Torsten Sattler, Marc Pollefeys, Esa Rahtu, and Juho Kannala. Dgc-net: Dense geometric correspondence network. In *WACV*, 2019.

[44] Lars Mescheder, Michael Oechsle, Michael Niemeyer, Sebastian Nowozin, and Andreas Geiger. Occupancy networks: Learning 3d reconstruction in function space. In *Proceedings of the IEEE/CVF Conference on Computer Vision and Pattern Recognition*, pages 4460–4470, 2019.

[45] Ben Mildenhall, Pratul P Srinivasan, Matthew Tancik, Jonathan T Barron, Ravi Ramamoorthi, and Ren Ng. Nerf: Representing scenes as neural radiance fields for view synthesis. In *European conference on computer vision*, pages 405–421. Springer, 2020.

[46] Juhong Min, Dahyun Kang, and Minsu Cho. Hypercorrelation squeeze for few-shot segmentation. *arXiv preprint arXiv:2104.01538*, 2021.

[47] Juhong Min, Seungwook Kim, and Minsu Cho. Convolutional hough matching networks for robust and efficient visual correspondence. *arXiv preprint arXiv:2109.05221*, 2021.

[48] Juhong Min, Jongmin Lee, Jean Ponce, and Minsu Cho. Hyperpixel flow: Semantic correspondence with multi-layer neural features. In *Proceedings of the IEEE/CVF International Conference on Computer Vision*, 2019.

[49] Juhong Min, Jongmin Lee, Jean Ponce, and Minsu Cho. Spair-71k: A large-scale benchmark for semantic correspondence. *arXiv preprint arXiv:1908.10543*, 2019.

[50] Juhong Min, Jongmin Lee, Jean Ponce, and Minsu Cho. Learning to compose hypercolumns for visual correspondence. In *Computer Vision–ECCV 2020: 16th European Conference, Glasgow, UK, August 23–28, 2020, Proceedings, Part XV 16*. Springer, 2020.

[51] Michael Niemeyer and Andreas Geiger. Giraffe: Representing scenes as compositional generative neural feature fields. In *Proceedings of the IEEE/CVF Conference on Computer Vision and Pattern Recognition*, pages 11453–11464, 2021.

[52] Michael Niemeyer, Lars Mescheder, Michael Oechsle, and Andreas Geiger. Differentiable volumetric rendering: Learning implicit 3d representations without 3d supervision. In *Proceedings of the IEEE/CVF Conference on Computer Vision and Pattern Recognition*, pages 3504–3515, 2020.

[53] Jeong Joon Park, Peter Florence, Julian Straub, Richard Newcombe, and Steven Lovegrove. Deepsdf: Learning continuous signed distance functions for shape representation. In *Proceedings of the IEEE/CVF Conference on Computer Vision and Pattern Recognition*, pages 165–174, 2019.

[54] Keunhong Park, Utkarsh Sinha, Jonathan T Barron, Sofien Bouaziz, Dan B Goldman, Steven M Seitz, and Ricardo Martin-Brualla. Nerfies: Deformable neural radiance fields. In *Proceedings of the IEEE/CVF International Conference on Computer Vision*, pages 5865–5874, 2021.

[55] Keunhong Park, Utkarsh Sinha, Peter Hedman, Jonathan T Barron, Sofien Bouaziz, Dan B Goldman, Ricardo Martin-Brualla, and Steven M Seitz. Hypernerf: A higher-dimensional representation for topologically varying neural radiance fields. *arXiv preprint arXiv:2106.13228*, 2021.

[56] Adam Paszke, Sam Gross, Soumith Chintala, Gregory Chanan, Edward Yang, Zachary DeVito, Zeming Lin, Alban Desmaison, Luca Antiga, and Adam Lerer. Automatic differentiation in pytorch. 2017.

[57] Songyou Peng, Michael Niemeyer, Lars Mescheder, Marc Pollefeys, and Andreas Geiger. Convolutional occupancy networks. In *European Conference on Computer Vision*, pages 523–540. Springer, 2020.

[58] Albert Pumarola, Enric Corona, Gerard Pons-Moll, and Francesc Moreno-Noguer. D-nerf: Neural radiance fields for dynamic scenes. In *Proceedings of the IEEE/CVF Conference on Computer Vision and Pattern Recognition*, pages 10318–10327, 2021.

[59] Daniel Rebain, Wei Jiang, Soroosh Yazdani, Ke Li, Kwang Moo Yi, and Andrea Tagliasacchi. Derf: Decomposed radiance fields. In *Proceedings of the IEEE/CVF Conference on Computer Vision and Pattern Recognition*, pages 14153–14161, 2021.

[60] Sashank J Reddi, Satyen Kale, and Sanjiv Kumar. On the convergence of adam and beyond. *arXiv preprint arXiv:1904.09237*, 2019.

[61] Christian Reiser, Songyou Peng, Yiyi Liao, and Andreas Geiger. Kilonerf: Speeding up neural radiance fields with thousands of tiny mlps. In *Proceedings of the IEEE/CVF International Conference on Computer Vision*, pages 14335–14345, 2021.

[62] Ignacio Rocco, Relja Arandjelovic, and Josef Sivic. Convolutional neural network architecture for geometric matching. In *CVPR*, 2017.

[63] Ignacio Rocco, Relja Arandjelović, and Josef Sivic. End-to-end weakly-supervised semantic alignment. In *CVPR*, 2018.

[64] Ignacio Rocco, Relja Arandjelović, and Josef Sivic. Efficient neighbourhood consensus networks via submanifold sparse convolutions. In *ECCV*, 2020.

[65] Ignacio Rocco, Mircea Cimpoi, Relja Arandjelović, Akihiko Torii, Tomas Pajdla, and Josef Sivic. Neighbourhood consensus networks. *arXiv preprint arXiv:1810.10510*, 2018.

[66] Edward Rosten and Tom Drummond. Machine learning for high-speed corner detection. In *European conference on computer vision*, pages 430–443. Springer, 2006.

[67] Michael Rubinstein, Armand Joulin, Johannes Kopf, and Ce Liu. Unsupervised joint object discovery and segmentation in internet images. In *CVPR*, 2013.

[68] Torsten Sattler, Bastian Leibe, and Leif Kobbelt. Efficient & effective prioritized matching for large-scale image-based localization. *IEEE transactions on pattern analysis and machine intelligence*, 39(9):1744–1756, 2016.

[69] Johannes L Schonberger and Jan-Michael Frahm. Structure-from-motion revisited. In *Proceedings of the IEEE conference on computer vision and pattern recognition*, pages 4104–4113, 2016.

[70] Katja Schwarz, Yiyi Liao, Michael Niemeyer, and Andreas Geiger. Graf: Generative radiance fields for 3d-aware image synthesis. *Advances in Neural Information Processing Systems*, 33:20154–20166, 2020.

[71] Paul Hongsuck Seo, Jongmin Lee, Deunsol Jung, Bohyung Han, and Minsu Cho. Attentive semantic alignment with offset-aware correlation kernels. In *Proceedings of the European Conference on Computer Vision (ECCV)*, pages 349–364, 2018.

[72] Karen Simonyan and Andrew Zisserman. Very deep convolutional networks for large-scale image recognition. *arXiv preprint arXiv:1409.1556*, 2014.

[73] Vincent Sitzmann, Julien Martel, Alexander Bergman, David Lindell, and Gordon Wetzstein. Implicit neural representations with periodic activation functions. *Advances in Neural Information Processing Systems*, 33:7462–7473, 2020.

[74] Matthew Tancik, Pratul Srinivasan, Ben Mildenhall, Sara Fridovich-Keil, Nithin Raghavan, Utkarsh Singhal, Ravi Ramamoorthi, Jonathan Barron, and Ren Ng. Fourier features let networks learn high frequency functions in low dimensional domains. *Advances in Neural Information Processing Systems*, 33:7537–7547, 2020.

[75] Tatsunori Taniai, Sudipta N Sinha, and Yoichi Sato. Joint recovery of dense correspondence and cosegmentation in two images. In *Proceedings of the IEEE conference on computer vision and pattern recognition*, pages 4246–4255, 2016.

[76] Prune Truong, Martin Danelljan, and Radu Timofte. Glu-net: Global-local universal network for dense flow and correspondences. In *Proceedings of the IEEE/CVF conference on computer vision and pattern recognition*, pages 6258–6268, 2020.

[77] Prune Truong, Martin Danelljan, Fisher Yu, and Luc Van Gool. Probabilistic warp consistency for weakly-supervised semantic correspondences. *arXiv preprint arXiv:2203.04279*, 2022.

[78] Ashish Vaswani, Noam Shazeer, Niki Parmar, Jakob Uszkoreit, Llion Jones, Aidan N Gomez, Łukasz Kaiser, and Illia Polosukhin. Attention is all you need. In *Advances in neural information processing systems*, 2017.

[79] Zirui Wang, Shangzhe Wu, Weidi Xie, Min Chen, and Victor Adrian Prisacariu. Nerf–: Neural radiance fields without known camera parameters. *arXiv preprint arXiv:2102.07064*, 2021.

[80] Alex Yu, Vickie Ye, Matthew Tancik, and Angjoo Kanazawa. pixelnerf: Neural radiance fields from one or few images. In *Proceedings of the IEEE/CVF Conference on Computer Vision and Pattern Recognition*, pages 4578–4587, 2021.

[81] Kai Zhang, Gernot Riegler, Noah Snavely, and Vladlen Koltun. Nerf++: Analyzing and improving neural radiance fields. *arXiv preprint arXiv:2010.07492*, 2020.

[82] Dongyang Zhao, Ziyang Song, Zhenghao Ji, Gangming Zhao, Weifeng Ge, and Yizhou Yu. Multi-scale matching networks for semantic correspondence. In *Proceedings of the IEEE/CVF International Conference on Computer Vision*, pages 3354–3364, 2021.

Checklist

1. For all authors...
   (a) Do the main claims made in the abstract and introduction accurately reflect the paper's contributions and scope? [Yes]
   (b) Did you describe the limitations of your work? [Yes]
   (c) Did you discuss any potential negative societal impacts of your work? [Yes] Supplementary material
   (d) Have you read the ethics review guidelines and ensured that your paper conforms to them? [Yes]
2. If you are including theoretical results...
   (a) Did you state the full set of assumptions of all theoretical results? [Yes]
   (b) Did you include complete proofs of all theoretical results? [N/A]
3. If you ran experiments...
   (a) Did you include the code, data, and instructions needed to reproduce the main experimental results (either in the supplemental material or as a URL)? [Yes] Psuedo-code will be provided in supplementary material.
   (b) Did you specify all the training details (e.g., data splits, hyperparameters, how they were chosen)? [Yes]
   (c) Did you report error bars (e.g., with respect to the random seed after running experiments multiple times)? [N/A]
   (d) Did you include the total amount of compute and the type of resources used (e.g., type of GPUs, internal cluster, or cloud provider)? [Yes] Supplementary material
4. If you are using existing assets (e.g., code, data, models) or curating/releasing new assets...
   (a) If your work uses existing assets, did you cite the creators? [Yes]
   (b) Did you mention the license of the assets? [N/A]
   (c) Did you include any new assets either in the supplemental material or as a URL? [N/A]
   (d) Did you discuss whether and how consent was obtained from people whose data you're using/curating? [N/A]
   (e) Did you discuss whether the data you are using/curating contains personally identifiable information or offensive content? [N/A]
5. If you used crowdsourcing or conducted research with human subjects...
   (a) Did you include the full text of instructions given to participants and screenshots, if applicable? [N/A]
   (b) Did you describe any potential participant risks, with links to Institutional Review Board (IRB) approvals, if applicable? [N/A]
   (c) Did you include the estimated hourly wage paid to participants and the total amount spent on participant compensation? [N/A]